Nature of Dynamical Coupling between Polarization and Strain in Nanoscale Ferroelectrics from First Principles

I. Ponomareva and L. Bellaiche

Department of Physics, University of Arkansas, Fayetteville, Arkansas 72701, USA

(Received 6 August 2008; published 6 November 2008)

A first-principle-based technique is used to investigate dynamical coupling between polarization and picosecond time-scale strain pulses in ferroelectric nanolayers. Two different dynamical mechanisms are found. The first mechanism concerns homogeneous dipole patterns, is governed by the ultrafast soft-mode dynamics, mostly consists in the modification of the dipoles' magnitude, and leads to a polarization only weakly changing and following the strain pulse via an ''usual'' coupling law. On the other hand, the second mechanism occurs in highly inhomogeneous dipole patterns, is characterized by a large change in polarization and by a time delay between polarization and strain, and is governed by the ''slower breathing'' of dipolar inhomogeneities. This second mechanism provides a successful explanation of puzzling experimental data.

DOI: 10.1103/PhysRevLett.101.197602 PACS numbers: 77.84.Dy, 78.20.Bh, 77.80.Dj

Ferroelectric nanostructures are of increasing interest due to their unique potential for the next generation of functional nanoscale devices with superior properties [1,2]. Recent studies have revealed unique features intrinsic to the nanoscale size [3–8]. Examples include nanostripe domains in ferroelectric ultrathin films [4,5], vortex states in ferroelectric nanodots [7], and different original ways to manipulate the chirality of such vortex states [9,10]. Another recent study discovered another intriguing behavior in low-dimensional ferroelectrics, that is the existence of a striking dynamical coupling between ferroelectric soft mode and uniaxal strain on a picosecond time scale in ferroelectric nanolayers [11]. More precisely, this latter, pioneering study was conducted on $Pb(Zr_{0.2}Ti_{0.8})O_3/SrRuO_3$ superlattices and revealed new exciting effects, such as (i) a time delay between the change in the tetragonal axial ratio associated with the uniaxial strain pulse and the corresponding soft-mode response; (ii) a huge reduction, and even annihilation, of the polarization; and (iii) a strong deviation from the usual coupling law between polarization and strain. These effects provide a new way to a controllable manipulation of the polarization on an ultrafast time scale, and thus open the way for the design of original, efficient devices. However, the mechanism responsible for such puzzling effects is a mystery, and their microscopic origins are completely unknown, to the best of our knowledge. Revealing such mechanism and origins is of obvious fundamental interest, and may also be the key to the engineering of materials with desirable, optimal properties. Here, we conduct first-principle-based simulations to investigate the nature of such dynamical coupling in nanoscale ferroelectrics. As we will see, a new phenomenon, which consists in the ''slow breathing'' of dipolar inhomogeneities, is discovered and explains all the experimental results of Ref. [11].

We simulate a thin film made of disordered $Pb(Zr_{0.4}Ti_{0.6})O_3$ (PZT), grown along the [001] pseudocubic direction (chosen to be the z axis), having PbO-terminated surfaces and interfaces and being 4.8 nm thick. Such film is modeled by $9.6\ \text{nm} \times 9.6\ \text{nm} \times 4.8\ \text{nm}$ supercells that are periodic along the x and y axes (which lie along the [100] and [010] pseudocubic directions, respectively) and finite along the z axis. The total energy of the film is given by

$$\mathcal{E}_{\text{tot}}(\mathbf{p_i}, \mathbf{v}_i, \eta, \sigma_i) = \mathcal{E}_{H_{\text{eff}}}(\mathbf{p_i}, \mathbf{v}_i, \eta, \sigma_i) + \frac{\beta}{2}\sum_i \langle \mathbf{E}_{\text{dep}} \rangle \cdot \mathbf{p_i}, \tag{1}$$

where $\mathbf{p_i}$ is the local dipole of the unit cell i of the film, while $\mathbf{v}_i$ is an inhomogeneous-strain-related variable in this unit cell i [12]. η is the homogeneous strain tensor and σ_i represents the atomic configuration of the solid solution [13]. The expression and first-principles-derived parameters of (the alloy effective Hamiltonian) $\mathcal{E}_{H_{\text{eff}}}$ energy are those given in Refs. [13] for PZT *bulk*, except for the dipole-dipole interactions for which we use the analytical expressions derived in Ref. [14] for thin films under ideal open-circuit (OC) conditions. The second term of Eq. (1) mimics a screening of the maximum depolarizing field inside the nanostructure, $\langle \mathbf{E}_{\text{dep}} \rangle$, with the magnitude of this screening being controlled by the β coefficient. $\beta = 1$ and $\beta = 0$ correspond to ideal short circuit (full screening of $\langle \mathbf{E}_{\text{dep}} \rangle$) and open circuit (no screening of $\langle \mathbf{E}_{\text{dep}} \rangle$) electrical boundary conditions, respectively. A value of β in-between describes a more realistic electrical boundary situation for which a residual depolarizing field exists inside the film [3]. Technically, $\langle \mathbf{E}_{\text{dep}} \rangle$ is calculated at an atomistic level [15]. Moreover, mechanical boundary conditions associated with epitaxial (001) films are also mimicked by freezing some components of the η strain tensor [5,16], namely $\eta_6 = 0$ and $\eta_1 = \eta_2 = \delta$, with δ characterizing the lattice mismatch between PZT and a chosen substrate. Here, we typically choose values of β slightly

smaller than 1 and $\delta = -1\%$ and also "play" with the time dependency of the η_3 component of the homogeneous strain tensor in order that our simulated setup is similar to the experimental situation of Ref. [11] in which compressively strained, 4.8 nm-thick (001) PZT nanolayers sandwiched by $SrRuO_3$ nanolayers are experiencing a time-dependent uniaxial strain along the [001] direction. The total energy $\mathcal{E}_{\text{tot}}$ is used in classical molecular dynamics (MD) simulations, with the Newton's equations of motion being solved for all the degrees of freedom included in the effective Hamiltonian approach. Note that combining first-principles-based effective Hamiltonian approaches with MD was found to accurately reproduce dynamics of perovskites [17]. The simulation temperature is set to $T = 300$ K.

As consistent with Ref. [5], several dipole patterns can develop in our investigated PZT film when varying the electrical boundary conditions while keeping the mechanical boundary unchanged. More precisely, the film develops a homogeneous domain pattern with all the dipoles pointing along the growth direction (pattern I) when $\beta > 0.97$, as a result of the static in-plane compressive strain (imposed by the substrate) that favors the formation of dipoles along the z direction [18]. On the other hand, for $\beta < 0.93$, the film exhibits the nanostripe domains experimentally found in Ref. [4] and alternating along the [010] direction with a periodicity of 4.8 nm (pattern II). Inside these domains, the dipoles either point "up" or "down" along the growth direction. Formation of such nanostripe domains results from the competition between the static in-plane compressive strain that favors the dipoles along the z direction and a large enough depolarizing field that disfavors configurations with nonzero z component of the total dipole moment. Moreover, in the intermediate region corresponding to $0.93 < \beta < 0.97$, *different* (meta)stable domain patterns are found, implying that several free-energy minima exist in that transitional region. Such (meta)stable patterns include patterns I and II, labyrinth structures, as well as original patterns (to be denoted as patterns III and IV) that we now describe in detail. In the pattern III, the so-called ferroelectric nanobubbles [19] form (that is, a small inclusion of dipoles pointing down develops inside a homogeneous configuration in which all the dipoles point up), with the density of 1 nanobubble per 92 nm^2. These nanobubbles have a size varying from 4.0 to 35.4 nm^3, and therefore occupy less than 8% of the total volume. Pattern III can thus be referred to as low-density nanobubbles, and is displayed in the leftmost frame of Fig. 2. On the other hand, pattern IV corresponds to nanobubbles with higher density. In this latter pattern, the density is of 1 nanobubble per 46 nm^2 and the size of the nanobubbles ranges between 55 to 84 nm^3. These nanobubbles therefore occupy 25%–38% of the film's volume. Pattern IV is visualized in the leftmost frame of Fig. 3. Note that these nanobubbles are typically found to adopt a cylindrical or spherical shape. Practically, all the (meta) stable domains associated with patterns III and IV were identified in a series of 180 simulations for which an initial inclusion of different size was first introduced inside a homogeneous dipole configuration and then the studied system was allowed to relax during 40 000–100 000 MD steps.

In the following, we chose $\beta = 0.94$ since it provides a realistic partial screening of polarization-induced surface charges in ultrathin nanostructures [3] and because of the associated variety of the dipole patterns described above. To study the dynamical coupling between an uniaxial strain applied along the growth direction and the soft mode, we first allow the chosen configuration to adopt its equilibrium axial ratio, τ_0, and average dipole moment, p_0, for $\beta = 0.94$ and $\delta = -1\%$. Then, an uniaxial time-dependent strain pulse with $\eta_3(t) = A\sin(2\pi\nu t - C)\exp^{-Bt} + D$ is applied along the film's growth direction at the time $t = t_0$. ν is the pulse frequency, A controls the pulse depth and B is responsible for the pulse decay. C and D are chosen such as to provide continuity of η_3 and $\partial\eta_3/\partial t$ at $t = t_0$. Figure 1(a) shows three different selected relative profiles for the $\frac{\tau(t)}{\tau(t_0)}$-versus-time curve, where $\tau(t) = \frac{1+\eta_3(t)}{1+\delta}$ is the c/a axial ratio (which is also denoted as the "tetragonality" in Ref. [11]), with the same frequency of 385 GHz. Note that the chosen $\tau(t)$ can be smaller from $\tau(t_0)$ by $\simeq 2\%$ at most. Figures 1(b)–1(d)

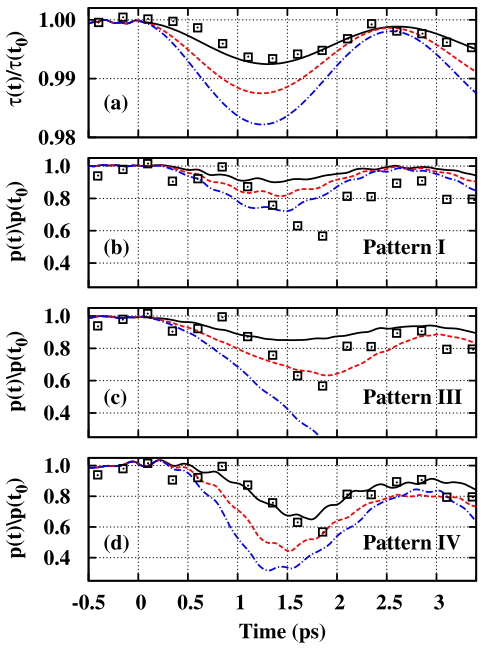

FIG. 1 (color online). Tetragonality [panel (a)] and average dipole moment [panels (b)–(d)], with respect to their equilibrium values, as a function of time for three different simulated dynamical strain pulses and in experiment. Lines show our predictions while the symbols represent the measurements of Ref. [11]. Simulation data in panels (b), (c), and (d) correspond to PZT thin films exhibiting the pattern I, pattern III with a nanobubble volume of 5.3 nm^3 and pattern IV with a nanobubble volume of 59.7 nm^3, respectively.

display the associated time evolution of the average electric dipole $p(t)$ when the film adopts pattern I, III, and IV, respectively. Note that (i) $p(t)$ provides a measure of the "soft mode displacement" introduced in Ref. [11]; and (ii) we do not report any data for pattern II and labyrinth structure since the average electric dipole vanishes for them. Data of Figs. 1(c) and 1(d) correspond to a nanobubble volume of 5.3 and 59.7 nm^3, respectively. Experimental data of Ref. [11] for compressively strained $Pb(Zr_{0.2}Ti_{0.8})O_3$ nanolayers are also shown in Figs. 1, for comparison. In particular, one can see that our strain pulse having the smallest depth is chosen to closely match the experimental one. Interestingly, different dipole patterns exhibit a qualitatively different response of the average dipole moment to the same applied strain. For pattern I, $p(t)$ follows any selected strain pulse with the "standard" coupling law of $[p(t)/p_0]^2 = [\tau(t) - \tau_C]/\tau_0$, where $\tau_0 = 1.038$ and $\tau_C = 0.963\tau_0$ is the so-called critical tetragonality [11]. As a result, there is no time delay between the minima of $\tau(t)$ and $p(t)$, and this latter quantity only decreases by up to $\simeq 10\%$ with respect to its initial value for our shallowest strain pulse—which contrasts with the $\simeq 50\%$ decrease of the soft-mode displacement observed in Ref. [11]. For the pattern III, the shallowest and intermediate strain pulse result in a minimal $p(t)/p(t_0)$ of 0.85 and 0.63, respectively, *and* of a time delay of 0.26 and 0.66 ps, respectively, between the minima of $p(t)$ and $\tau(t)$. Moreover, for this pattern III, the deepest strain pulse leads to a full vanishing (with no further recovering) of the polarization when the tetragonality becomes equal to 98.2% of its initial value, which is a striking phenomenon that has also been experimentally observed [11] (note also that this critical value of 0.982 for $\frac{\tau}{\tau(t_0)}$ is very close to the experimental value of 0.979 for the ratio between the critical tetragonality and initial tetragonality [11]). Regarding pattern IV, our data are in excellent agreement with experiment for the weakest strain pulse both for the time delay and reduction of $p(t)$ (note also that the initial tetragonality for pattern IV is found to be $\simeq 1.033$, which is consistent with the experimental value of 1.042 reported in Ref. [11], especially when realizing that the grown sample has a Ti composition larger by 0.2 from our simulated system). As the applied compressive strain becomes deeper, Fig. 1(d) shows that $p(t)$ reduces even more but the polarization never fully vanishes, unlike for pattern III. In fact, we investigated 28 different configurations possessing different nanobubbles' sizes, and never found a complete annihilation of the polarization for the three considered strain pulses but rather a maximal reduction of the dipole moment by 80%. Our calculations further reveal that a time delay also exists between the minima of $p(t)$ and $\tau(t)$ for pattern IV. The most striking findings evidenced by Figs. 1 are that the average dipole moment (i) can be greatly reduced by a picosecond time-scale strain pulse, (ii) exhibits a time delay with respect to the applied strain pulse, and therefore (iii) strongly deviates from the "usual" law of $(p/p_0)^2 = (\tau - \tau_C)/\tau_0$ in the inhomogeneous patterns III and IV, unlike in the homogeneous pattern I. To understand the origin for such different behaviors, we decided to inspect the evolution of the local dipole pattern as a function of the applied strain.

For pattern I, the behavior of the dipole moment shown in Fig. 1(b) mostly originates from the strain-induced change of the dipoles' *magnitude*. The dynamics of such change is governed by the soft-mode characteristic frequency [20], which explains why $p(t)$ follows $\tau(t)$, when this latter varies on a picosecond time scale in a homogeneous pattern [21]. Moreover, snapshots of the dipole configuration at different times are shown in Fig. 2 for the pattern III associated with the macroscopic results displayed in Fig. 1(c) for the intermediate strain pulse. The nanobubble continuously grows in size when $0.00 < t < 1.96$ ps and then progressively shrinks in size when $1.96 < t < 3.00$ ps, while the magnitude of the uniaxial compressive strain first increases between $0.00 < t < 1.30$ ps before decreasing when $1.30 < t < 2.60$ ps. Practically, at $t = 1.96$ ps, the volume of the nanobubble has increased by almost 9 times with respect to its initial value, as a result of the *flip* from the up to the down direction of $\simeq 700$ dipoles located near the nanobubble boundary (wall). Such considerable change in the nanobubble volume caused by the dipoles' flip explains the large decrease of the average dipole moment found for pattern III. To understand why the flip occurs near the nanobubble wall one has to consider the local environment of the flipping dipole. If a down dipole is surrounded by down dipoles only (as in case of monodomain) then it will be energetically costly for such dipole to complete a jump to the up state. Or likewise, for the up dipole surrounded by the up neighbors it is energetically costly to complete a jump to the down state. Around the nanobubble boundary, however, a dipole is both surrounded by up and down neighbors. Because of such interesting surrounding, the dipoles near the nanobubble wall can relatively easily accomplish both jumps from the up to the down direction and from the down to the up direction. As a result, the

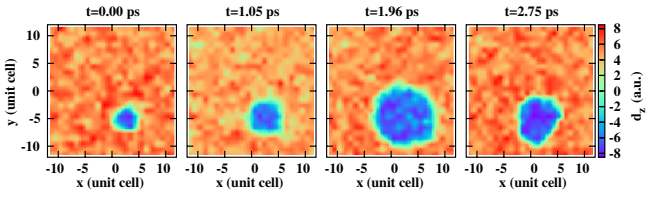

FIG. 2 (color online). Snapshots at different times of a (x, y) cross section of the dipole pattern in a PZT film initially possessing low-density nanobubbles (pattern III). This cross section corresponds to the most inner (001) B plane, and the x and y axis lie along the [100] and [010] directions, respectively. Red (respectively, blue) areas show areas with dipoles pointing up (respectively, down) along the z direction. These data correspond to the intermediate strain pulse [dashed lines in Figs. 1(a) and 1(c)], and an initial nanobubble volume of 5.3 nm^3.

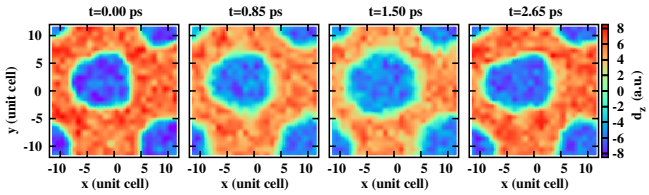

FIG. 3 (color online). Same as Fig. 2 but for pattern IV (high-density nanobubbles) with an initial nanobubble volume of 59.7 nm^3.

nanobubble wall mobility is large enough ($\approx$510 m/s, or equivalently 5.1 Å/ps, for its radial velocity in case of the intermediate strain) to allow the nanobubbles to change in size on an ultrafast time scale. However, such velocity is not large enough to allow $p(t)$ to precisely follow $\tau(t)$ on a picosecond time scale, which therefore explains why there is a time delay of the order of tenths of ps between the minima of $\tau(t)$ and $p(t)$ for pattern III [22]. For the pattern IV associated with Fig. 1(d), a detailed inspection of the dipole pattern as a function of time reveals that the ''breathing'' of the nanobubbles is also the primordial dynamical mechanism, as in pattern III, which therefore explains both the large reduction and time delay of $p(t)$ in pattern IV. Interestingly, the average radial velocity of the nanobubbles wall under the intermediate strain pulse is equal to 5.6 Å/ps for the pattern IV of Fig. 3, and is therefore similar to the one corresponding to pattern III of Fig. 2, while their relative maximal reductions in polarization are rather different [see Figs. 1(c) and 1(d) for the intermediate strain pulse]. Such difference arises from the fact that pattern IV has a smaller initial polarization, as a result of bigger and denser nanobubbles.

In summary, we used first-principle-based simulations to reveal the atomistic nature(s) of the dynamical coupling between ferroelectric soft mode and uniaxial strain in ferroelectric nanolayers. We found two different coupling mechanisms depending on the kind of dipole pattern in the nanolayers. For homogeneous dipole patterns, the coupling is governed by the ultrafast soft-mode dynamics through a reduction of the dipole magnitudes whereas for inhomogeneous patterns the coupling occurs through nanobubble's ''breathing'' (the change of nanobubble size due to nanobubble wall dynamics). This latter mechanism provides a successful explanation for recent puzzling and technologically promising observations of a large dynamical change, and time delay, of the polarization [11].

We acknowledge support from NSF Grants No. DMR-0080054 (C-SPIN), No. DMR-0701558, and No. DMR-0404335, ONR Grants No. N00014-04-1-0413 and No. N00014-08-1-0915, and DOE Grant No. DE-FG02-05ER46188.

[1] J. F. Scott and C. A. P. de Araujo, Science **246**, 1400 (1989).
[2] J. F. Scott, J. Phys. Condens. Matter **18**, R361 (2006).
[3] J. Junquera and P. Ghosez, Nature (London) **422**, 506 (2003).
[4] D. Fong, G. Stephenson, S. Streier, J. Eastman, O. Auciello, P. Fuoss, and C. Thompson, Science **304**, 1650 (2004).
[5] I. Kornev, H. Fu, and L. Bellaiche, Phys. Rev. Lett. **93**, 196104 (2004).
[6] I. Ponomareva and L. Bellaiche, Phys. Rev. B **74**, 064102 (2006).
[7] I. Naumov, L. Bellaiche, and H. Fu, Nature (London) **432**, 737 (2004).
[8] H. Fu and L. Bellaiche, Phys. Rev. Lett. **91**, 257601 (2003).
[9] S. Prosandeev, I. Ponomareva, I. Kornev, I. Naumov, and L. Bellaiche, Phys. Rev. Lett. **96**, 237601 (2006).
[10] S. Prosandeev, I. Ponomareva, I. Kornev, and L. Bellaiche, Phys. Rev. Lett. **100**, 047201 (2008).
[11] C. v. Korff Schmising, M. Bargheer, M. Kiel, N. Zhavoronkov, M. Woerner, T. Elsaesser, I. Vrejoiu, D. Hesse, and M. Alexe, Phys. Rev. Lett. **98**, 257601 (2007).
[12] W. Zhong, D. Vanderbilt, and K. M. Rabe, Phys. Rev. B **52**, 6301 (1995).
[13] L. Bellaiche, A. Garcia, and D. Vanderbilt, Phys. Rev. Lett. **84**, 5427 (2000).
[14] I. Naumov and H. Fu, arXiv:cond-mat/0505497.
[15] I. Ponomareva, I. I. Naumov, I. Kornev, H. Fu, and L. Bellaiche, Phys. Rev. B **72**, 140102(R) (2005).
[16] N. A. Pertsev, V. G. Kukhar, H. Kohlstedt, and R. Waser, Phys. Rev. B **67**, 054107 (2003).
[17] I. Ponomareva, L. Bellaiche, T. Ostapchuk, J. Hlinka, and J. Petzelt, Phys. Rev. B **77**, 012102 (2008).
[18] N. A. Pertsev, A. G. Zembilgotov, and A. K. Tagantsev, Phys. Rev. Lett. **80**, 1988 (1998).
[19] B.-K. Lai, I. Ponomareva, I. I. Naumov, I. Kornev, H. Fu, L. Bellaiche, and G. J. Salamo, Phys. Rev. Lett. **96**, 137602 (2006).
[20] For $PbZr_{0.4}Ti_{0.6}O_3$ the calculated A1 mode characteristic frequency at $T = 300$ K is 200 cm^{-1} which is about 25% higher than the experimental value [V. Sivasubramaniany, V. Murthyy, B. Viswanathanz, and M. Sieskindx, J. Phys. Condens. Matter **8**, 2447 (1996)]. This overestimation does not, however, significantly affect the results reported in this Letter as verified by performing a separate set of calculations where the soft-mode mass was rescaled to bring the A1 mode frequency in agreement with the experimental value. Note also that both simulation and this experiment by Sivasubramaniany *et al.* indicate that the A1 mode is underdamped at this temperature.
[21] A tiny fraction of dipoles ($<$0.4%) also begins to *flip* from the ''up'' to the ''down'' direction for the shallowest investigated strain pulse in pattern I. Additional Monte Carlo simulations we performed strongly suggests that such dipole flipping is a general mechanism to accumulate large compressive uniaxial strains in homogeneously polarized epitaxial films.
[22] Our calculations indicate that the polarization dynamics away from the nanobubble walls is associated with the variation of dipoles' magnitude governed by the ultrafast soft-mode dynamics whereas polarization dynamics at the nanobubble walls is dominated by the variation of dipoles' direction, or dipole flipping, governed by the relatively slow mobility of the domain walls. The overall polarization variation is a sum of these two contributions.